NASA/TM-20240004143

Out of Plane Stresses Using a Beam-Based Elastic Foundation Bonded Joint Model

Scott E. Stapleton
University of Massachusetts Lowell, Lowell, Massachusetts

Brett A. Bednarcyk and Evan J. Pineda
Glenn Research Center, Cleveland, Ohio

Andrew C. Bergan
Langley Research Center, Hampton, Virginia

April 2024

NASA STI Program Report Series

Since its founding, NASA has been dedicated to the advancement of aeronautics and space science. The NASA scientific and technical information (STI) program plays a key part in helping NASA maintain this important role.

The NASA STI program operates under the auspices of the Agency Chief Information Officer. It collects, organizes, provides for archiving, and disseminates NASA's STI. The NASA STI program provides access to the NTRS Registered and its public interface, the NASA Technical Reports Server, thus providing one of the largest collections of aeronautical and space science STI in the world. Results are published in both non-NASA channels and by NASA in the NASA STI Report Series, which includes the following report types:

- TECHNICAL PUBLICATION.
  Reports of completed research or a major significant phase of research that present the results of NASA Programs and include extensive data or theoretical analysis. Includes compilations of significant scientific and technical data and information deemed to be of continuing reference value. NASA counterpart of peer-reviewed formal professional papers but has less stringent limitations on manuscript length and extent of graphic presentations.

- TECHNICAL MEMORANDUM.
  Scientific and technical findings that are preliminary or of specialized interest, e.g., quick release reports, working papers, and bibliographies that contain minimal annotation. Does not contain extensive analysis.

- CONTRACTOR REPORT.
  Scientific and technical findings by NASA-sponsored contractors and grantees.

- CONTRACTOR REPORT.
  Scientific and technical findings by NASA-sponsored contractors and grantees.

- CONFERENCE PUBLICATION.
  Collected papers from scientific and technical conferences, symposia, seminars, or other meetings sponsored or co-sponsored by NASA.

- SPECIAL PUBLICATION.
  Scientific, technical, or historical information from NASA programs, projects, and missions, often concerned with subjects having substantial public interest.

- TECHNICAL TRANSLATION.
  English-language translations of foreign scientific and technical material pertinent to NASA's mission.

Specialized services also include organizing and publishing research results, distributing specialized research announcements and feeds, providing information desk and personal search support, and enabling data exchange services.

For more information about the NASA STI program, see the following:

- Access the NASA STI program home page at http://www.sti.nasa.gov

NASA/TM-20240004143

Out of Plane Stresses Using a Beam-Based Elastic Foundation Bonded Joint Model

Scott E. Stapleton
University of Massachusetts Lowell, Lowell, Massachusetts

Brett A. Bednarcyk and Evan J. Pineda
Glenn Research Center, Cleveland, Ohio

Andrew C. Bergan
Langley Research Center, Hampton, Virginia

National Aeronautics and
Space Administration

Glenn Research Center
Cleveland, Ohio 44135

April 2024

Acknowledgments

This work was funded under the NASA Space Technologies Mission Directorate Thermoplastics Development for Exploration Applications (TDEA) project and the NASA Exploration Systems Mission Directorate Space Launch Systems (SLS) Universal Stage Adapter (USA) project.

Level of Review: This material has been technically reviewed by technical management.

This report is available in electronic form at https://www.sti.nasa.gov/ and https://ntrs.nasa.gov/

NASA STI Program/Mail Stop 050
NASA Langley Research Center
Hampton, VA 23681-2199

Out of Plane Stresses Using a Beam-Based Elastic Foundation Bonded Joint Model

Scott E. Stapleton
University of Massachusetts Lowell
Lowell, Massachusetts 01854

Brett A. Bednarcyk and Evan J. Pineda
National Aeronautics and Space Administration
Glenn Research Center
Cleveland, Ohio 44135

Andrew C. Bergan
National Aeronautics and Space Administration
Langley Research Center
Hampton, Virginia 23681–2199

Abstract

Efficient, semi-analytical models of bonded joints are utilized for initial joint design and sizing due to their convenience and speed. Many of these models are based on beam and plate theories, which are most applicable when in-plane stresses/strains dominate. While this can be a sensible assumption for obtaining the deformations of the joint, out of plane (transverse) stresses are often of critical importance for failure in bonded joints composed of fiber reinforced composite materials. Since through-thickness strains are neglected in these semi-analytical theories, the present study shows a method to back-calculate the out of plane stresses based on stress balance equations, which use the in-plane stresses and displacements that have already been obtained. The method was implemented within the Joint Element Designer (JED) software, and verification and validation examples have been shown. As is typical for these types of models, corner stress singularities are not captured by the JED model, but the general trends of the stress and deformation fields agreed with a higher fidelity finite element model. As such, this method for obtaining out of plane stresses, when coupled with the JED code, is very useful for the complete stress analysis of bonded composite joints.

Introduction

While detailed finite element models are the dominant high fidelity method of analyzing bonded joints, semi-analytical design models are still utilized in early design phases (Refs. 1 and 2). While these models almost always carry with them geometrical and material restrictions (as all structural models do), they can still accommodate a wide variety of joint geometries. The present study highlights the advancements for one of these models, the Joint Element Designer (JED) (Refs. 3 and 4). This model was originally created to represent adhesively bonded joints, where the bondline is thin. Based on a finite element formulation with shape functions specialized to represent a semi-analytic joint solution, JED treated the adherends as beams, while the adhesive was represented as a bed of springs joining the adherends. The adhesive utilized a linear interpolation of the displacement field from one adherend to the other, and a semi-numerical method was used to solve the system of ODEs to obtain the axial function of centerline displacements. More recently, this formulation was altered to accommodate joints including

sandwich panel cores. For a sandwich core, a linear displacement field through the thickness is often not sufficient to represent the dissipation of displacements in the core. Therefore, a node was added in the core, and a quadratic displacement field through the thickness in the core was assumed. These JED joint elements can be joined via nodes like standard finite elements, but have higher order shape functions which allow one element through the thickness and often very few along the length. As such, JED can provide detailed predictions of bonded joint stress/strain fields with orders of magnitude fewer elements compared to standard continuum-based finite element models. Additional features such as offset joining and rotation about nodes were added to accommodate the many styles of joint found in practice.

Even though in-plane axial stresses energetically dominate the response of a double lap joint, failure in fiber reinforced composites is often initiated from out of plane normal and shear stresses arising from the joint's discontinuous geometry and cause delamination and transverse cracking. Therefore, to fully analyze the joint, a method of estimating these stresses needs to be developed and integrated into any structural joint model such as the Joint Element Developer (JED).

In this study, a formulation is first presented for extracting out of plane stresses from the predicted joint displacement fields. These stresses usually can be neglected when formulating the strain energy because they are usually relatively small compared to axial stresses, but the tendency of fiber reinforced composite joints to fail in delamination and transverse cracking makes the estimation of these stresses critical. Second, a double lap sandwich joint, which was modelled as a sub-model in a larger component model using a traditional 3-D continuum finite element technique, will be compared with a JED model: tips and tricks of the modeling will be discussed, and differences will be highlighted.

Out of Plane Stresses: Formulation

Plates under cylindrical bending are assumed to have strain only in the axial *x*-direction. From this strain, in-plane stresses such as normal stress in the *x* and *y*-directions, σ_{xx} and σ_{yy}, along with shear stresses in the *xy* plane, τ_{xy}, can be directly obtained from their relationship with the axial strain. However, the out of plane (transverse) stresses, τ_{xz}, σ_{zz} and τ_{yz}, cannot be directly obtained. As shown below, by considering the equilibrium equations, the transverse stresses can be estimated based on the in-plane stress components (Ref. 5). These can then be used for failure predictions in the beam formulations for the adherends.

Euler-Bernoulli Beam Formulation

For a composite plate under cylindrical bending with generalized plane strain, the strains, using Euler-Bernoulli beam theory, can be written as:

$$\varepsilon_{xx} = u' - zw'' \text{ and } \varepsilon_{yy} = \hat{\varepsilon}_{yy} \tag{1}$$

where u and w are the plate centerline axial and transverse displacements of the beam (functions of *x*), $\blacksquare'$ is the derivative with respect to *x*, and $\hat{\varepsilon}_{yy}$ is the constant width-direction plane strain. The stresses in the *k*th ply of the *i*th adherend can then be defined as:

$$\begin{aligned} {\sigma_{xx}}^k &= \bar{Q}^k_{11}\varepsilon_{xx} + \bar{Q}^k_{12}\varepsilon_{yy}, \\ {\sigma_{yy}}^k &= \bar{Q}^k_{21}\varepsilon_{xx} + \bar{Q}^k_{22}\varepsilon_{yy}, \text{ and} \\ {\tau_{xy}}^k &= \bar{Q}^k_{13}\varepsilon_{xx} + \bar{Q}^k_{23}\varepsilon_{yy}. \end{aligned} \tag{2}$$

The superscript *i* for the adherend has been temporarily dropped for simplicity but will be introduced later. Additionally, the local *z* axis for adherend *i*, z_i, (Figure 1) will be introduced later.

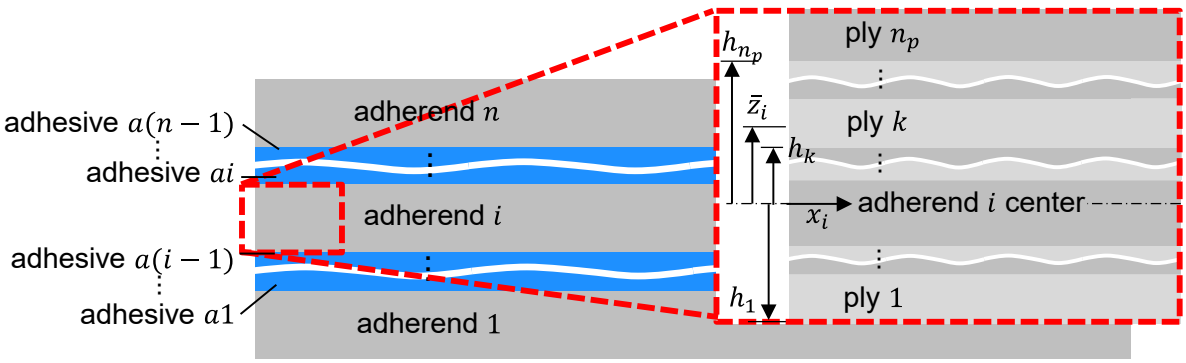

Figure 1.—Numbering of an n adherends with adhesive between them, and each ply has n_p plies with an adherend coordinate system and ply coordinate system.

Shear stress, τ_{xz}

Starting with the x-direction, equilibrium in terms of stresses can be written as:

$$\frac{\partial \sigma_{xx}^k}{\partial x} + \frac{\partial \tau_{xy}^k}{\partial y} + \frac{\partial \tau_{xz}^k}{\partial z} = 0, \tag{3}$$

and due to the assumption of cylindrical bending, which means the stresses are independent of the y-direction, Equation (3) can be reduced to,

$$\frac{\partial \sigma_{xx}^k}{\partial x} + \frac{\partial \tau_{xz}^k}{\partial z} = 0. \tag{4}$$

To solve for the shear stress, τ_{xz}^k, at a point within ply k, $(x, \bar{z})$, we can integrate over z in the ply from the lower bound of the ply, h_k, to $\bar{z}$:

$$\int_{h_k}^{\bar{z}} \frac{\partial \tau_{xz}^k}{\partial z} dz = -\int_{h_k}^{\bar{z}} \frac{\partial \sigma_{xx}^k}{\partial x} dz. \tag{5}$$

The integral on the left-hand side of the equation can be performed and rearranged to get:

$$\tau_{xz}^k(\bar{z}) = \tau_{xz}^k(h_k) - \int_{h_k}^{\bar{z}} \frac{\partial \sigma_{xx}^k}{\partial x} dz. \tag{6}$$

Now, consider the second term on the right-hand side of Equation (6). The differential of the axial stress, σ_{xx}^k, can be taken in terms of the centerline displacements from Equations (2) and (1) to obtain,

$$\frac{\partial \sigma_{xx}^k}{\partial x} = \bar{Q}_{11}^k (u'' - zw''') \tag{7}$$

and then the integral can be applied to obtain,

$$\int_{h_k}^{\bar{z}} \frac{\partial \sigma_{xx}^k}{\partial x} dz = \bar{Q}_{11}^k \left(zu'' - \frac{1}{2} z^2 w''' \right) \Big|_{h_k}^{\bar{z}}. \tag{8}$$

Evaluating the right-hand side of Equation (8) at the bounds gives,

$$\int_{h_k}^{\bar{z}} \frac{\partial \sigma_{xx}^k}{\partial x} dz = \bar{Q}_{11}^k \left((\bar{z} - h_k) u'' - \frac{1}{2} (\bar{z}^2 - h_k^2) w''' \right) \tag{9}$$

which we will write as,

$$\int_{h_k}^{\bar{z}} \frac{\partial \sigma_{xx}^k}{\partial x} dz = \bar{Q}_{11}^k f(\bar{z}, h_k, x) \tag{10}$$

where,

$$f(\bar{z}, h_k, x) = (\bar{z} - h_k)u'' - \frac{1}{2}\left(\bar{z}^2 - h_k^2\right)w'''. \tag{11}$$

Finally, the shear stress becomes,

$$\tau_{xz}^k(\bar{z}) = \tau_{xz}^k(h_k) - \bar{Q}_{11}^k f(\bar{z}, h_k, x). \tag{12}$$

Because the shear stress is continuous in the *z*-direction, the stress at the bottom of the *k*th ply is the same as the stress at the top of ply (*k* - 1),

$$\tau_{xz}^k(h_k) = \tau_{xz}^{k-1}(h_k). \tag{13}$$

Equation (12) can be repeated for the (*k*-1)th ply to get

$$\tau_{xz}^{k-1}(h_k) = \tau_{xz}^{k-1}(h_{k-1}) - \bar{Q}_{11}^{k-1} f(h_k, h_{k-1}, x)\,. \tag{14}$$

Finally, this can be used for each ply until the bottom ply is reached to get a new version of Equation (12):

$$\tau_{xz}^k(\bar{z}) = \tau_{xz}^1(h_1) - \bar{Q}_{11}^k f(\bar{z}, h_k, x) - \sum_{n=2}^{k}\left(\bar{Q}_{11}^{n-1} f(h_n, h_{n-1}, x)\right). \tag{15}$$

Now, in context of the joint element formulation, the *x* coordinate is common for the entire element, and $\bar{z}_i$ is the z coordinate in the local coordinate system centered in adherend *i*. In full notation, the shear stress in adherend *i*, ${}_i\tau_{xz}^k(\bar{z}_i)$, can be written as

$${}_i\tau_{xz}^k(\bar{z}_i) = {}_{ai}\tau_{xy}\left({}_{ai}h_1\right) - {}_i\bar{Q}_{11}^k f\left(\bar{z}_i,\ {}_ih_k, x\right) - \sum_{n=2}^{k}\left(\ {}_i\bar{Q}_{11}^{n-1} f\left(\ {}_ih_n,\ {}_ih_{n-1}, x\right)\right). \tag{16}$$

where ${}_{ai}\tau_{xy}\left({}_{ai}h_1\right)$ is the shear stress at the top of the adhesive below the adherend. If the adherend does not have adhesive below it (*i* = 1), the shear stress below is 0 and Equation (16) reduces to

$${}_i\tau_{xz}^k(\bar{z}_i) = -\ {}_i\bar{Q}_{11}^k f\left(\bar{z}_i,\ {}_ih_k, x\right) - \sum_{n=2}^{k}\left(\ {}_i\bar{Q}_{11}^{n-1} f\left(\ {}_ih_n,\ {}_ih_{n-1}, x\right)\right). \tag{17}$$

This gives an equation for the shear stress at each point in the adherend. This conversion can be done on any of the stress components derived below in the same way. For practical application, the centerline displacements and their derivatives can be obtained using the solution of the governing equations already calculated at a single location *x* (Ref. 3). Additionally, the stresses at the border of each ply can be calculated once and used for multiple z coordinates to save on computational time.

Normal Stress, σ_{zz}

Considering the z-direction, equilibrium in terms of stresses can be written as:

$$\frac{\partial \sigma_{zz}^k}{\partial z} + \frac{\partial \tau_{yz}^k}{\partial y} + \frac{\partial \tau_{xz}^k}{\partial x} = 0, \tag{18}$$

and due to the assumption of cylindrical bending, this equation reduces to,

$$\frac{\partial \sigma_{zz}^k}{\partial z} + \frac{\partial \tau_{xz}^k}{\partial x} = 0. \tag{19}$$

To solve for the normal (peel) stress, σ_{zz}^k, at a point $(x, z = \bar{z})$ in ply k, we can integrate over z in the ply from the lower bound of the ply, h_k, to $\bar{z}$:

$$\int_{h_k}^{\bar{z}} \frac{\partial \sigma_{zz}^k}{\partial z} dz = -\int_{h_k}^{\bar{z}} \frac{\partial \tau_{xz}^k}{\partial x} dz. \tag{20}$$

The integral on the left-hand side of the equation can be performed and rearranged to obtain:

$$\sigma_{zz}^k(\bar{z}) = \sigma_{zz}^k(h_k) - \int_{h_k}^{\bar{z}} \frac{\partial \tau_{xz}^k}{\partial x} dz. \tag{21}$$

Now, consider the second term on the right-hand side. An expression for the shear stress can be taken from Equation (15) and differentiated with respect to x to obtain,

$$\frac{\partial \tau_{xz}^k}{\partial x} = {\tau_{xz}^1}'(h_1) - \bar{Q}_{11}^k f'(z, h_k, x) - \sum_{n=2}^{k} \left(\bar{Q}_{11}^{n-1} f'(h_n, h_{n-1}, x) \right) \tag{22}$$

where,

$$f'(z, h_k, x) = (z - h_k)u''' - \frac{1}{2}\left(z^2 - h_k^2\right)w''''. \tag{23}$$

Here, only $f'(z, h_k, x)$ is a function of z, so the integration can be applied, and the equation can be slightly rearranged to obtain,

$$\int_{h_k}^{\bar{z}} \frac{\partial \tau_{xz}^k}{\partial x} dz = (\bar{z} - h_k)\left({\tau_{xz}^1}'(h_1) - \sum_{n=2}^{k} \left(\bar{Q}_{11}^{n-1} f'(h_n, h_{n-1}, x) \right) \right) - \bar{Q}_{11}^k \int_{h_k}^{\bar{z}} f'(z, h_k, x) dz \tag{24}$$

where,

$$\int_{h_k}^{\bar{z}} f'(z, h_k, x) dz = \left(\frac{1}{2} z^2 - h_k z \right)_{h_k}^{\bar{z}} u''' - \frac{1}{2}\left(\frac{1}{3} z^3 - h_k^2 z \right)_{h_k}^{z} w'''' \tag{25}$$

which evaluates to,

$$\int_{h_k}^{\bar{z}} f'(z, h_k, x) dz = \left(\frac{1}{2}\bar{z}^2 - \bar{z}h_k + \frac{1}{2}h_k^2 \right) u''' - \frac{1}{2}\left(\frac{1}{3}\bar{z}^3 - \bar{z}h_k^2 + \frac{2}{3}h_k^3 \right) w''''. \tag{26}$$

This can be substituted into Equation (21) to obtain,

$$\sigma_{zz}^{k}(\bar{z}) = \sigma_{zz}^{k}(h_k) - (\bar{z} - h_k)\left(\tau_{xz}^{1}{}'(h_1) - \sum_{2}^{n=k}\left(\bar{Q}_{11}^{n-1} f(h_n, h_{n-1}, x)\right)\right) + \bar{Q}_{11}^{k}\int_{h_k}^{\bar{z}} f'(z, h_k, x)dz. \quad (27)$$

Finally, the stress component from the previous ply is found in terms the ply before, until the first ply is reached. This combined with the full notation introduced in Equation (17) gives the relation:

$$\begin{gathered} {}_{i}\sigma_{zz}^{k}(\bar{z}) = {}_{i}\sigma_{zz}^{k}(h_1) - \left[(\bar{z}_{\iota} - h_k) + \sum_{2}^{n=k}(h_n - h_{n-1})\right]\Big[\ {}_{i}\tau_{xz}^{1}{}'(h_1) - \\ \sum_{n=2}^{k}\Big(\ {}_{i}\bar{Q}_{11}^{n-1} f'(h_n, h_{n-1}, x)\Big)\Big] + \ {}_{i}\bar{Q}_{11}^{k}\int_{h_k}^{\bar{z}} f'(z, h_k, x)dz + \\ \sum_{n=2}^{k}\Big(\ {}_{i}\bar{Q}_{11}^{n-1}\int_{h_{n-1}}^{h_n} f'(h_n, h_{n-1}, x)dz\Big). \end{gathered} \quad (28)$$

Shear stress, τ_{yz}

Considering the *y*-direction, equilibrium in terms of stresses can be written as:

$$\frac{\partial \tau_{xy}^{k}}{\partial x} + \frac{\partial \sigma_{yy}^{k}}{\partial y} + \frac{\partial \tau_{yz}^{k}}{\partial z} = 0, \quad (29)$$

And, once again, due to the assumption of cylindrical bending, this equation reduces to,

$$\frac{\partial \tau_{xy}^{k}}{\partial x} + \frac{\partial \tau_{yz}^{k}}{\partial z} = 0. \quad (30)$$

To solve for the shear stress, τ_{yz}^{k}, at a point $(x, z = \bar{z})$ within ply k, we can integrate over z in the ply from the lower bound of the ply, h_k, to $\bar{z}$:

$$\int_{h_k}^{\bar{z}} \frac{\partial \tau_{yz}^{k}}{\partial z} dz = -\int_{h_k}^{\bar{z}} \frac{\partial \tau_{xy}^{k}}{\partial x} dz. \quad (31)$$

The integral on the left-hand side of Equation (31) can be performed and rearranged to obtain:

$$\tau_{yz}^{k}(\bar{z}) = \tau_{yz}^{k}(h_k) - \int_{h_k}^{\bar{z}} \frac{\partial \tau_{xy}^{k}}{\partial x} dz. \quad (32)$$

Now, consider the second term on the right-hand side. Using Equation (11), we obtain,

$$\int_{h_k}^{\bar{z}} \frac{\partial \tau_{xy}^{k}}{\partial x} dz = \bar{Q}_{13}^{k} f(\bar{z}, h_k, x). \quad (33)$$

Finally, the shear stress becomes,

$$\tau_{yz}^{k}(\bar{z}) = \tau_{yz}^{k}(h_k) - \bar{Q}_{13}^{k} f(\bar{z}, h_k, x). \quad (34)$$

As before, this relation can be cascaded to the bottom ply (ply 1) which allows us to write in full notation:

$$\tau_{yz}^{k}(\bar{z}) = \tau_{yz}^{1}(h_1) - \bar{Q}_{13}^{k} f(\bar{z}_{\iota}, h_k, x) - \sum_{n=2}^{k}\left(\bar{Q}_{13}^{n-1} f(h_n, h_{n-1}, x)\right). \quad (35)$$

Currently, there are no *yz* shear stresses in the adhesive nor at the bottom surface of the bottom adherend, so in full notation, the equation simplifies to

$$ {}_i\tau_{yz}^k(\bar{z}_i) = -\ {}_i\bar{Q}_{13}^k f(\bar{z}_i, h_k, x) - \sum_{n=2}^{k}\left({}_i\bar{Q}_{13}^{n-1} f(h_n, h_{n-1}, x)\right). \tag{36} $$

Timoshenko Beam Formulation

This formulation follows beam theory for classical lamination theory (CLT), where shear deformations are considered in equilibrium. The strains involved include axial, shear, and generalized plane strain as:

$$ \begin{aligned} \varepsilon_{xx} &= u' + z\psi', \\ \gamma_{xz} &= w' - \psi, \\ \varepsilon_{yy} &= \hat{\varepsilon}_{yy} \end{aligned} \tag{37} $$

where ψ is the rotation due to bending of the beam as a function of *x*. The stresses for the *k*th ply can then be written as:

$$ \begin{aligned} {\sigma_{xx}}^k &= \bar{Q}_{11}^k\varepsilon_{xx} + \bar{Q}_{12}^k\varepsilon_{yy}, \\ {\tau_{xy}}^k &= \bar{Q}_{13}^k\varepsilon_{xx} + \bar{Q}_{23}^k\varepsilon_{yy}, \\ {\sigma_{yy}}^k &= \bar{Q}_{21}^k\varepsilon_{xx} + \bar{Q}_{22}^k\varepsilon_{yy}, \\ {\tau_{xz}}^k &= k_s\bar{Q}_{66}^k\gamma_{xz}. \end{aligned} \tag{38} $$

The variable k_s represents the shear correction factor commonly used in shear deformation beam theory, where k_s = 5/6 is commonly used for rectangular cross-sections. This factor attempts to account for the fact that the shear stress is overpredicted because the theory assumes constant shear in the layer, whereas actual beams have a parabolic stress distribution through the thickness.

Normal Stress, σ_{zz}

Considering the *z*-direction, equilibrium terms of stresses can be written as:

$$ \frac{\partial\sigma_{zz}^k}{\partial z} + \frac{\partial\tau_{yz}^k}{\partial y} + \frac{\partial\tau_{xz}^k}{\partial x} = 0, \tag{39} $$

and due to the assumption of cylindrical bending, this reduces to,

$$ \frac{\partial\sigma_{zz}^k}{\partial z} + \frac{\partial\tau_{xz}^k}{\partial x} = 0. \tag{40} $$

To solve for the normal (peel) stress, σ_{zz}^k, at a point $(x, \bar{z})$ within ply *k* , we can integrate over *z* in the ply from the lower bound of the ply, h_k, to $\bar{z}$:

$$ \int_{h_k}^{\bar{z}} \frac{\partial\sigma_{zz}^k}{\partial z}\,dz = -\int_{h_k}^{\bar{z}} \frac{\partial\tau_{xz}^k}{\partial x}\,dz. \tag{41} $$

The integral on the left-hand side of Equation (41) can be performed and rearranged to get:

$$ \sigma_{zz}^k(\bar{z}) = \sigma_{zz}^k(h_k) - \int_{h_k}^{\bar{z}} \frac{\partial\tau_{xz}^k}{\partial x}\,dz. \tag{42} $$

Now, consider the second term on the right-hand side. The expression for the shear stress and strain can be taken from Equations (37) and (38), and differentiation with respect to *x* yields,

$$\frac{\partial \tau_{xz}^k}{\partial x} = k_s \bar{Q}_{66}^k g(z, h_k, x) \tag{43}$$

where,

$$g(z, h_k, x) = (z - h_k)(w'' - \psi'). \tag{44}$$

Finally, the peel stress becomes,

$$\sigma_{zz}^k(\bar{z}) = \sigma_{zz}^k(h_k) - k\bar{Q}_{66}^k g(z, h_k, x). \tag{45}$$

As before, this relation can be cascaded to the bottom ply (ply 1), which allows us to write in full notation:

$${}_i\sigma_{zz}^k(\bar{z}_i) = {}_i\sigma_{zz}^1(h_k) - k\ {}_i\bar{Q}_{66}^k g(\bar{z}_i, h_k, x) - \sum_{n=2}^{k}\left(k\ {}_i\bar{Q}_{66}^k g(\bar{z}_i, h_k, x)\right). \tag{46}$$

The peel stress at the bottom of the adherend is either 0 if it is the last ply or the value of the peel stress at the adhesive below the current adherend.

Shear stress, τ_{yz}

Considering the *y*-direction, equilibrium in terms of stresses can be written as:

$$\frac{\partial \tau_{xy}^k}{\partial x} + \frac{\partial \sigma_{yy}^k}{\partial y} + \frac{\partial \tau_{yz}^k}{\partial z} = 0, \tag{47}$$

and due to the assumption of cylindrical bending, this reduces to

$$\frac{\partial \tau_{xy}^k}{\partial x} + \frac{\partial \tau_{yz}^k}{\partial z} = 0. \tag{48}$$

To solve for the shear stress, τ_{yz}^k, at a point $(x, z = \bar{z})$ within ply *k*, we can integrate over *z* in the ply from the lower bound of the ply, h_k, to $\bar{z}$:

$$\int_{h_k}^{\bar{z}} \frac{\partial \tau_{yz}^k}{\partial z} dz = -\int_{h_k}^{\bar{z}} \frac{\partial \tau_{xy}^k}{\partial x} dz. \tag{49}$$

The integral on the left-hand side of Equation (49) can be performed and rearranged to obtain:

$$\tau_{yz}^k(\bar{z}) = \tau_{yz}^k(h_k) - \int_{h_k}^{\bar{z}} \frac{\partial \tau_{xy}^k}{\partial x} dz. \tag{50}$$

Now, consider the second term on the right-hand side. Using the expression for the shear stress and strain can from Equations (37) and (38), yields

$$\int_{h_k}^{\bar{z}} \frac{\partial \tau_{xy}^k}{\partial x} dz = \bar{Q}_{13}^k f_2(\bar{z}, h_k, x) \tag{51}$$

where,

$$f_2(z, h_k, x) = (\bar{z} - h_k)u'' + \frac{1}{2}(\bar{z}^2 - h_k^2)\psi''. \tag{52}$$

Finally, the shear stress becomes,

$$\tau_{yz}^k(\bar{z}) = \tau_{yz}^k(h_k) - \bar{Q}_{13}^k f_2(\bar{z}, h_k, x). \tag{53}$$

Once again, this relation can be cascaded to the bottom ply (ply 1) which allows us to write:

$$\tau_{yz}^k(\bar{z}) = \tau_{yz}^1(h_1) - \bar{Q}_{13}^k f_2(\bar{z}, h_k, x) - \sum_{n=2}^{k} \left(\bar{Q}_{13}^{n-1} f_2(h_n, h_{n-1}, x)\right). \tag{54}$$

Currently, there are no *yz* shear stresses in the adhesive nor at the bottom surface, so in full notation Equation (54) simplifies to,

$${}_i\tau_{yz}^k(\bar{z}_i) = - {}_i\bar{Q}_{13}^k f(\bar{z}_i, h_k, x) - \sum_{n=2}^{k} \left({}_i\bar{Q}_{13}^{n-1} f_2(h_n, h_{n-1}, x)\right). \tag{55}$$

Verification

Two single element verification models were created to test the functionality of the above formulation and to check that the out of plane stresses generally allow stress continuity between plies and layers, along with stress-free boundaries.

The first example in Figure 2 is a 3-layered joint element with transversely isotropic adherends (shown in gray) and two adhesive layers (shown in blue) joining the adherends. The input file with the geometries, material properties, and boundary conditions is given in the Appendix. No units were used as this was to be a purely numeric example. As can be seen from the plots in Figure 2, the example has verified that: shear stress is continuous between adhesive and adherend layers, and that the tops and bottoms are generally stress free as can be expected. Even though the integration occurs from the top down, the stress is still very close to zero at the bottom surface.

The second example (Figure 3) has isotropic adherends (shown in gray) and a core (shown in blue) rather than adhesive. For the core formulation, an extra node is found in the layer allowing the displacements through the thickness. This example highlights some deficiencies in the model for a sandwich core. The stresses are continuous between an adherend and the core below it because the integration starts at the bottom and goes up, so continuity is enforced in this direction. However, there is a slight lack of continuity between the adherend and core above it. This may be due to lack of accuracy in the numerical derivative. This appears to be the case for all stress components examined here. This warrants further work to investigate whether this is due to a numerical inaccuracy, bug in the implementation, or flawed assumption in the formulation.

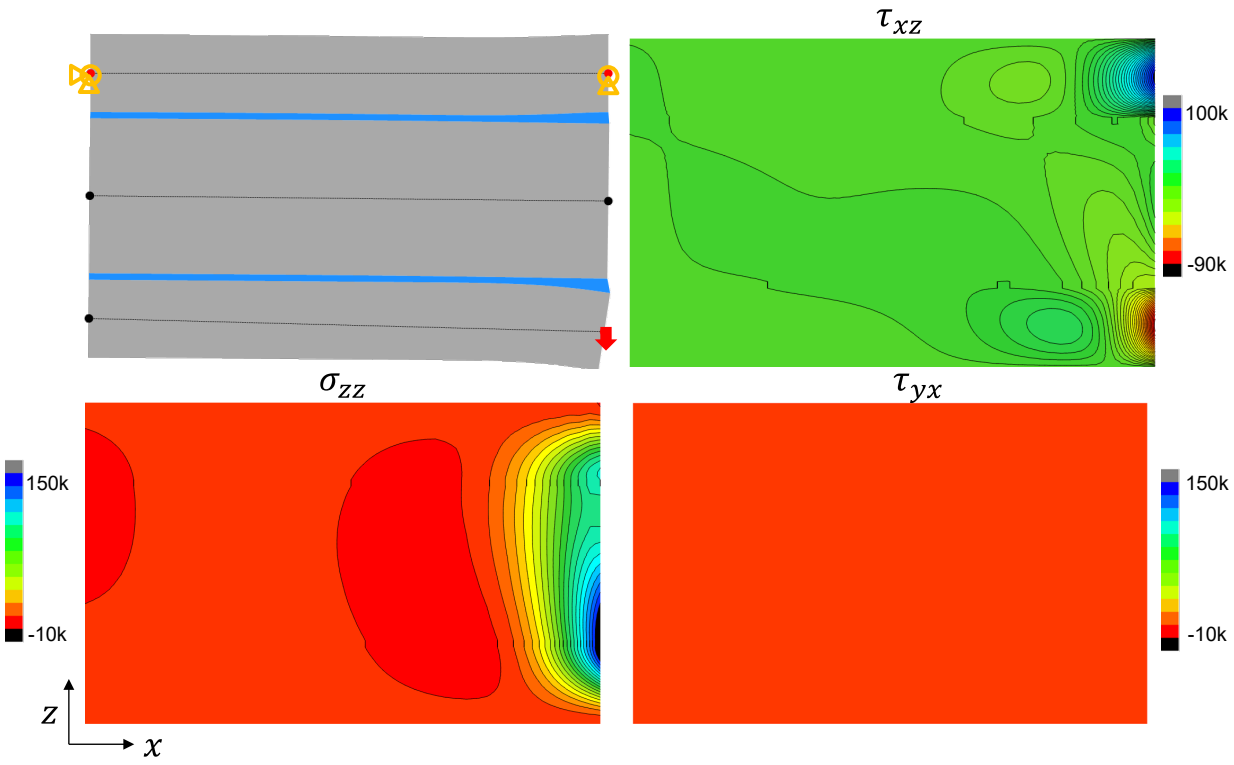

Figure 2.—Verification example for three composite adherends (gray) with adhesive layers (blue) in between each, showing the out-of-plane stresses and their continuity between layers.

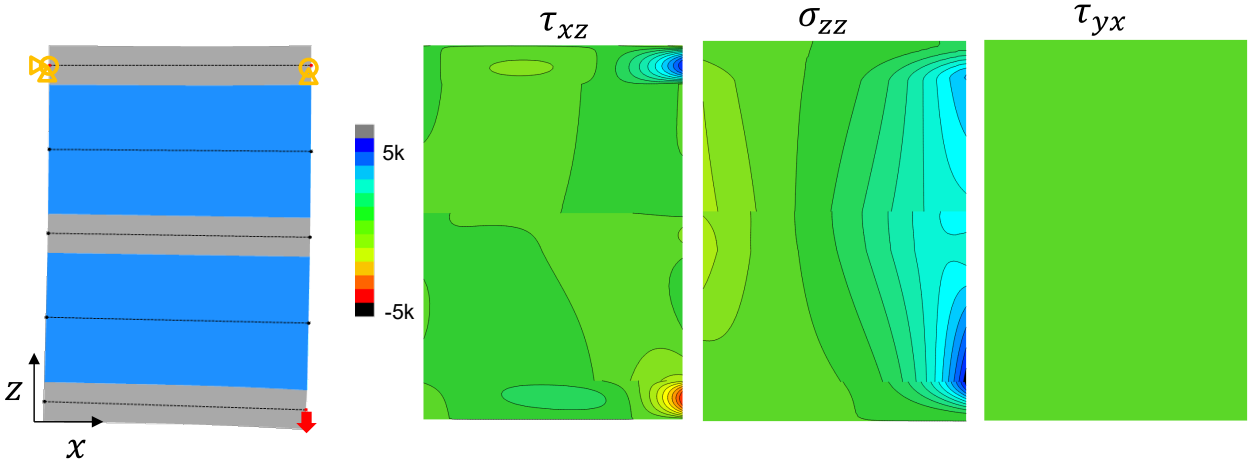

Figure 3.—Verification example for three isotropic adherends (gray) with sandwich cores (blue) connecting them all, showing the out-of-plane stresses and their slight discontinuity between layers.

Validation

For validation with a 3D dense-meshed continuum-based finite element model, the reader is directed to the publication “A Critical Assessment of Design Tools for Stress Analysis of Adhesively Bonded Double Lap Joints” by Stapleton et al. (Ref. 2). In this study, the out-of-plane and axial stresses are compared for five double lap joints of progressive complication. A joint with homogeneous adherends, composite adherends, composite adherends with ply drops, and all these variations with a sandwich core were compared. In general, the adherend out-of-plane stresses were fairly well represented, with discrepancies between the JED model and dense continuum finite element model occurring mainly at reentrant corners. While these regions are indeed critical, the accuracy was considered acceptable for a design-type model like JED, where some fidelity is traded for computational speed and ease-of-use.

Summary

In this study, a formulation for calculating the out-of-plane stresses from a cylindrical bending bonded joint design model was given, and verification and validation examples were shown. The in-plane stresses of the adherends were used in the main JED formulation and to solve for equilibrium, since these stresses are most often dominant. The out of plane stresses were obtained by applying the stress equilibrium equations in the adherends and integrating per ply from the lower surfaces. Two verification examples were presented to show the out of plane stresses and continuity between the adherends and the adhesive. The adhesive model performed as expected, but the sandwich model exhibited slight discontinuity between layers due to lack of accuracy in the numerical derivativer, which would make the solution different depending on the direction of integration. This did not influence the in-plane stresses, but rather only the out of plane stresses.

For validation, another work was cited (Ref. 2). In general, the JED predictions were in good agreement with those of a continuum finite element model. However, it was shown that the stress singularities at sharp reentrant corners predicted by the continuum finite element model were not represented by the plate-based JED model, as one would expect. It is questionable whether such singularities occur in real joints , and these singularities predicted by finite element models are usually highly mesh-dependent and thus there absolute magnitudes are usually not used in strength predictions.

Appendix

Verification Example 1:

```
*Materials
0,Aluminum,TransIsotropic,1200000, 800000, 451128, 0.33
1,Adhesive,Isotropic,133000, 50000
**
*XSections
0, DoubleAdherend, 1.0, Uniform, 0.06, Aluminum
1, SingleAdherend, 1.0, Laminate, 3, 0/ 90 / 15, Aluminum / Aluminum / Aluminum, 0.04 / 0.04 /0.04 /
2, Adhesive, 1.0, Uniform, 0.005, Adhesive
**
*Segments
0, DLJ, 0.4, 3, DoubleAdherend /SingleAdherend /DoubleAdherend /, Adhesive /Adhesive /, 0
**
*Instances
0,DLJ,0 - 5
**
*DOF Nodes
0,0
0,3
0,5
**
*BCs
Uz,0,0,0,
Thetay,0,0,0,
Ux,0,0,0,
Uz,0,0,3,
Thetay,0,0,3,
Uz,-0.01,0,5,
*END
```

Verification Example 2:

```
*Materials
0,Aluminum,TransIsotropic,1200000, 1200000, 451128, 0.33
1,Adhesive,Isotropic,133000, 50000
**
*XSections
0, SingleAdherend, 1.0, Uniform, 0.06, Aluminum
1, DoubleAdherend, 1.0, Uniform, 0.06, Aluminum
2, Adhesive, 1.0, Uniform, 0.2, Adhesive
**
*Segments
0, DLJ, 0.4, 3, DoubleAdherend /SingleAdherend /DoubleAdherend /, Adhesive /Adhesive/,6
**
*Instances
0,DLJ,0 – 5
**
*DOF Nodes
0,00,5
0,9
**
*BCs
Uz,0,0,0,
Thetay,0,0,0,
Ux,0,0,0,
Uz,0,0,5,
Thetay,0,0,5,
Uz,-0.01,0,9,
*END
```

The input file for the initial coarse JED model prior to full linking of nodes together:

```
*Materials
**
**Number, Name, Type
**Isotropic: E,G,(optional)CTE
**Transversely Isotropic: E11,E22,G12,Nu12,(optional)Nu23, CTE11, CTE22
**
0,Facesheet,TransIsotropic,11500000, 11748000, 3443300, 0.3519
1,Core,TransIsotropic,45000, 100, 13000, 0.001
2,Doubler,TransIsotropic,10489000, 10756000, 3766000, 0.4141
3,Adhesive,Isotropic,500000, 192000
4,GapFiller,Isotropic,610000, 217857
**
*XSections
**
**Number, Name, Width, Type (Uniform or Laminate),(Uniform: Thickness, Material)(Laminate: # of Plys,
     Orientation, Material, Ply Thickness (sep by /)
**
0, Facesheet, 1, Laminate, 6, 0/0/0/0/0/0/, Facesheet/Facesheet/Facesheet/Facesheet/Facesheet/Facesheet/,
     0.010643333/0.010643333/0.010643333/0.010643333/0.010643333/0.010643333/
1, Core, 1, Uniform, 1.351, Core
2, DoublerTop, 1, Laminate, 13, 0/0/0/0/0/0/0/0/0/0/0/0/0/,
     Doubler/Doubler/Doubler/Doubler/Doubler/Doubler/Doubler/Facesheet/Facesheet/Facesheet/Facesheet/Faces
     heet/Facesheet/,
     0.01071/0.01071/0.01071/0.01071/0.01071/0.01071/0.01071/0.010643333/0.010643333/0.010643333/0.0106433
     33/0.010643333/0.010643333/
3, DoublerBottom, 1, Laminate, 13, 0/0/0/0/0/0/0/0/0/0/0/0/0/,
     Facesheet/Facesheet/Facesheet/Facesheet/Facesheet/Facesheet/Doubler/Doubler/Doubler/Doubler/Doubler/D
     oubler/Doubler/,
     0.010643333/0.010643333/0.010643333/0.010643333/0.010643333/0.010643333/0.01071/0.01071/0.01071/0.010
     71/0.01071/0.01071/0.01071/
4, TaperTop_1, 1, Laminate, 7, 0/0/0/0/0/0/0/,
     Doubler/Facesheet/Facesheet/Facesheet/Facesheet/Facesheet/Facesheet/,
     0.01071/0.010643333/0.010643333/0.010643333/0.010643333/0.010643333/0.010643333/
5, TaperTop_2, 1, Laminate, 8, 0/0/0/0/0/0/0/0/,
     Doubler/Doubler/Facesheet/Facesheet/Facesheet/Facesheet/Facesheet/Facesheet/,
     0.01071/0.01071/0.010643333/0.010643333/0.010643333/0.010643333/0.010643333/0.010643333/
6, TaperTop_3, 1, Laminate, 9, 0/0/0/0/0/0/0/0/0/,
     Doubler/Doubler/Doubler/Facesheet/Facesheet/Facesheet/Facesheet/Facesheet/Facesheet/,
     0.01071/0.01071/0.01071/0.010643333/0.010643333/0.010643333/0.010643333/0.010643333/0.010643333/
7, TaperTop_4, 1, Laminate, 10, 0/0/0/0/0/0/0/0/0/0/,
     Doubler/Doubler/Doubler/Doubler/Facesheet/Facesheet/Facesheet/Facesheet/Facesheet/Facesheet/,
     0.01071/0.01071/0.01071/0.01071/0.010643333/0.010643333/0.010643333/0.010643333/0.010643333/0.0106433
     33/
8, TaperTop_5, 1, Laminate, 11, 0/0/0/0/0/0/0/0/0/0/0/,
     Doubler/Doubler/Doubler/Doubler/Doubler/Facesheet/Facesheet/Facesheet/Facesheet/Facesheet/Facesheet/,
     0.01071/0.01071/0.01071/0.01071/0.01071/0.010643333/0.010643333/0.010643333/0.010643333/0.010643333/0
     .010643333/
9, TaperTop_6, 1, Laminate, 12, 0/0/0/0/0/0/0/0/0/0/0/0/,
     Doubler/Doubler/Doubler/Doubler/Doubler/Doubler/Facesheet/Facesheet/Facesheet/Facesheet/Facesheet/Fac
     esheet/,
     0.01071/0.01071/0.01071/0.01071/0.01071/0.01071/0.010643333/0.010643333/0.010643333/0.010643333/0.010
     643333/0.010643333/
10, TaperBottom_1, 1, Laminate, 7, 0/0/0/0/0/0/0/,
     Facesheet/Facesheet/Facesheet/Facesheet/Facesheet/Facesheet/Doubler/,
     0.010643333/0.010643333/0.010643333/0.010643333/0.010643333/0.010643333/0.01071/
11, TaperBottom_2, 1, Laminate, 8, 0/0/0/0/0/0/0/0/,
     Facesheet/Facesheet/Facesheet/Facesheet/Facesheet/Facesheet/Doubler/Doubler/,
     0.010643333/0.010643333/0.010643333/0.010643333/0.010643333/0.010643333/0.01071/0.01071/
```

```
12, TaperBottom_3, 1, Laminate, 9, 0/0/0/0/0/0/0/0/0/,
     Facesheet/Facesheet/Facesheet/Facesheet/Facesheet/Facesheet/Doubler/Doubler/Doubler/,
     0.010643333/0.010643333/0.010643333/0.010643333/0.010643333/0.010643333/0.01071/0.01071/0.01071/
13, TaperBottom_4, 1, Laminate, 10, 0/0/0/0/0/0/0/0/0/0/,
     Facesheet/Facesheet/Facesheet/Facesheet/Facesheet/Facesheet/Doubler/Doubler/Doubler/Doubler/,
     0.010643333/0.010643333/0.010643333/0.010643333/0.010643333/0.010643333/0.01071/0.01071/0.01071/0.010
     71/
14, TaperBottom_5, 1, Laminate, 11, 0/0/0/0/0/0/0/0/0/0/0/,
     Facesheet/Facesheet/Facesheet/Facesheet/Facesheet/Facesheet/Doubler/Doubler/Doubler/Doubler/Doubler/,
     0.010643333/0.010643333/0.010643333/0.010643333/0.010643333/0.010643333/0.01071/0.01071/0.01071/0.010
     71/0.01071/
15, TaperBottom_6, 1, Laminate, 12, 0/0/0/0/0/0/0/0/0/0/0/0/,
     Facesheet/Facesheet/Facesheet/Facesheet/Facesheet/Facesheet/Doubler/Doubler/Doubler/Doubler/Doubler/D
     oubler/,
     0.010643333/0.010643333/0.010643333/0.010643333/0.010643333/0.010643333/0.01071/0.01071/0.01071/0.010
     71/0.01071/0.01071/
16, Adhesive, 1, Uniform, 0.005, Adhesive
17, Gap, 1, Uniform, 0.005, GapFiller
18, DoublerOnlyTop, 1, Laminate, 7, 0/0/0/0/0/0/0/,
     Doubler/Doubler/Doubler/Doubler/Doubler/Doubler/Doubler/,
     0.01071/0.01071/0.01071/0.01071/0.01071/0.01071/0.01071/
19, DoublerOnlyBottom, 1, Laminate, 7, 0/0/0/0/0/0/0/,
     Doubler/Doubler/Doubler/Doubler/Doubler/Doubler/Doubler/,
     0.01071/0.01071/0.01071/0.01071/0.01071/0.01071/0.01071/
10, , 1, Uniform, 1.47872, GapFiller
**
*Segments
**
**Number, Name, Length, Number of Adherends, Adherends (sep. by /), Adhesives (sep. by /), Model
     Type(0=UncoupledShear, 1=CoupledShear, 2=UncoupledShearPlusAxial, 3=LinearPlaneStrain,
     4=TimoshenkoUncoupled, 5=Frostig, 6=QuadraticUncoupled, 7=QuadraticPlaneStrain,
     8=QuadraticPlaneStress, 9=TimoshenkoQuadPlaneStrain, 10=IsotropicQuadUncoupled, )
**
0, Sandwich, 2, 2, Facesheet /Facesheet /, Core /, 6
1, Taper1, 0.3936, 2, TaperTop_1 /TaperBottom_1 /, Core /, 6
2, Taper2, 0.3936, 2, TaperTop_2 /TaperBottom_2 /, Core /, 6
3, Taper3, 0.3936, 2, TaperTop_3 /TaperBottom_3 /, Core /, 6
4, Taper4, 0.3936, 2, TaperTop_4 /TaperBottom_4 /, Core /, 6
5, Taper5, 0.3936, 2, TaperTop_5 /TaperBottom_5 /, Core /, 6
6, Taper6, 0.3936, 2, TaperTop_6 /TaperBottom_6 /, Core /, 6
7, Doubler, 1.20515, 2, DoublerTop /DoublerBottom /, Core /, 6
8, Gap, 0.2065, 2, DoublerOnlyTop / DoublerOnlyBottom/, , 6
**
*Instances
**
**Number, Segment Name, Nodes (numbered from upper-left, down, then over), Optional: Optional:
     Rotation(deg, CW) / Node about which to rotate
**
0,Sandwich,0 - 5
1,Taper1,0 - 5
2,Taper2,0 - 5
3,Taper3,0 - 5
4,Taper4,0 - 5
5,Taper5,0 - 5
6,Taper6,0 - 5
7,Doubler,0 - 5
8,Gap,0 - 5
9,Doubler,0 - 5
10,Taper6,0 - 5
11,Taper5,0 - 5
12,Taper4,0 - 5
13,Taper3,0 - 5
```

```
14,Taper2,0 - 5
15,Taper1,0 - 5
16,Sandwich,0 - 5
**
*Linked Nodes
**
**Node 1, Instance #, Node # , Node 2: Instance #, Node #, Offset or Alignment(Center, Top, Bottom)
**
Node 1, 0,3,Node 2, 1,0,Bottom
Node 1, 1,3,Node 2, 2,0,Bottom
Node 1, 2,3,Node 2, 3,0,Bottom
Node 1, 3,3,Node 2, 4,0,Bottom
Node 1, 4,3,Node 2, 5,0,Bottom
Node 1, 5,3,Node 2, 6,0,Bottom
Node 1, 6,3,Node 2, 7,0,Bottom
Node 1, 7,3,Node 2, 8,0,Top
Node 1, 8,3,Node 2, 9,0,Top
Node 1, 9,3,Node 2, 10,0,Bottom
Node 1, 10,3,Node 2, 11,0,Bottom
Node 1, 11,3,Node 2, 12,0,Bottom
Node 1, 12,3,Node 2, 13,0,Bottom
Node 1, 13,3,Node 2, 14,0,Bottom
Node 1, 14,3,Node 2, 15,0,Bottom
Node 1, 15,3,Node 2, 16,0,Bottom
**
*DOF Nodes
**
**Node Instance #, Instance Node #
**
0,0
0,1
0,2
16,3
16,5
**
*Loads
**
**Type (Fx,Fz,My), Magnitude, Point: Instance, Node
**
Fx,1373.25,16,3,
Fx,1373.25,16,5,
**
*BCs
**
**Type (Ux,Uz,Thetay), Magnitude, Point: Instance, Node
**
Ux,0,0,0,
Thetay,0,0,0,
Ux,0,0,1,
Thetay,0,0,1,
Ux,0,0,2,
Uz,0,0,2,
Thetay,0,0,2,
Thetay,0,16,3,
Thetay,0,16,5,
**
*END
```

References

1. S.E. Stapleton et al., “Comparison of Design Tools for Stress Analysis of Adhesively Bonded Joints,” in AIAA Scitech 2019 Forum, San Diego, CA: American Institute of Aeronautics and Astronautics, Jan. 2019. doi: 10.2514/6.2019-0232.
2. S.E. Stapleton et al., “A critical assessment of design tools for stress analysis of adhesively bonded double lap joints,” Mechanics of Advanced Materials and Structures, vol. 28, no. 8, pp. 791–811, Jun. 2019, doi: 10.1080/15376494.2019.1600768.
3. S.E. Stapleton and A.M. Waas, “The analysis of adhesively bonded advanced composite joints using joint finite elements,” Glenn Research Center, Cleveland, Ohio, NASA/CR—2012-217606, 2012.
4. S.E. Stapleton, E.J. Pineda, T. Gries, and A.M. Waas, “Adaptive shape functions and internal mesh adaptation for modeling progressive failure in adhesively bonded joints,” International Journal of Solids and Structures, doi: 10.1016/j.ijsolstr.2014.05.022.
5. J. Zhang, B.A. Bednarcyk, C.S. Collier, P.W. Yarrington, Y. Bansal, and M.-J. Pindera, “Analysis Tools for Adhesively Bonded Composite Joints, Part 2: Unified Analytical Theory,” AIAA Journal, vol. 44, no. 8, pp. 1709–1719, Aug. 2006, doi: 10.2514/1.15664.